Domain stability of $PbTiO_3$ thin films under anisotropic misfit strains: Phase-field simulations

G. Sheng,[1,a)] J. X. Zhang,[1] Y. L. Li,[1] S. Choudhury,[1] Q. X. Jia,[2] Z. K. Liu,[1] and L. Q. Chen[1]
[1]*Department of Materials Science and Engineering, The Pennsylvania State University, University Park, Pennsylvania 16802, USA*
[2]*MPA-STC, Los Alamos National Laboratory, Los Alamos, New Mexico 87545, USA*

(Received 26 June 2008; accepted 1 July 2008; published online 5 September 2008)

The domain stability and domain structures of (001)-oriented $PbTiO_3$ ferroelectric thin films subject to anisotropic in-plane strains were studied using phase-field method. Based on the simulation results, a room temperature domain/phase stability diagram was constructed for $PbTiO_3$ thin films with the in-plane strains ranging from −5% to 5%. The predicted diagram is both quantitatively and qualitatively different from those obtained using thermodynamic calculations based on a single-domain assumption. © *2008 American Institute of Physics*. [DOI: 10.1063/1.2974093]

I. INTRODUCTION

$PbTiO_3$ is a prototypic ferroelectric perovskite and a component for a number of important piezoelectric solid-solution systems including $PbZrO_3$-$PbTiO_3$ (PZT), $Pb(Zn_{1/3}Nb_{2/3})O_3$-$PbTiO_3$ (PZN-PT), and $Pb(Mg_{1/3}Nb_{2/3})O_3$-$PbTiO_3$ (PMN-PT). The phase transition behavior in a bulk $PbTiO_3$ single crystal is relatively simple; it exhibits a single transition from paraelectric cubic phase to ferroelectric tetragonal phase. However, the phase transition may become more complicated in a thin film state. It has been shown theoretically[1–4] as well as experimentally[5–7] that epitaxial strains may lead to different equilibrium domain states from the corresponding bulk and the ferroelectric transition temperature can be raised by hundreds of degrees by either tensile or compressive biaxial strains.

The thermodynamics of strain effect on phase transitions in ferroelectric thin films was pioneered by Pertsev *et al.*[1] who published the first misfit strain–temperature diagram for $PbTiO_3$ under a symmetrical biaxial strain and a single-domain assumption for all the possible ferroelectric states. However, significantly different domain stability diagrams[1,3,8–10] were obtained if one considers the possibility of domain structure formation under symmetrical biaxial strains. More recently, the isothermal "misfit strain–misfit strain" domain stability diagrams under anisotropic biaxial strains were constructed for $PbTiO_3$ films using thermodynamic calculations under a single-domain assumption.[11–14] Therefore, the main objective of this work is to construct a "misfit strain–misfit strain" domain stability diagram for $PbTiO_3$ thin films by taking into account three-dimensional domain structures. For this purpose, we employ the phase-field approach for ferroelectric phase transitions and domain structures in thin films.

II. SIMULATION DETAILS

We consider a (001)-oriented $PbTiO_3$ thin film on an orthorhombic substrate, i.e., under anisotropic misfit strains. A rectangular coordinate system, $\boldsymbol{x}=(x_1,x_2,x_3)$ is set up with the x_1, x_2 and x_3 axes along the [100], [010] and [001] crystallographic directions, respectively. The ferroelectric domain structure is described by the spatial distribution of the spontaneous polarization vector $\boldsymbol{P}(\boldsymbol{x})=(P_1,P_2,P_3)$. The temporal evolution of $\boldsymbol{P}$ and the domain structures are governed by the time-dependent Ginzburg–Landau (TDGL) equations,

$$\frac{\partial P_i(\boldsymbol{x},t)}{\partial t} = -L\frac{\delta F}{\delta P_i(\boldsymbol{x},t)}, \quad i=1,2,3, \tag{1}$$

where L is the kinetic coefficient related to the domain wall mobility, and F is the total free energy of the system. $\delta F/\delta P_i(\boldsymbol{x},t)$ is the thermodynamic driving force for the spatial and temporal evolution of $P_i(\boldsymbol{x},t)$. The total free energy F includes the bulk free energy, elastic deformation energy, domain wall energy and electrostatic energy, i.e.,

$$F = \int_V [f_{\text{bulk}}(P_i) + f_{\text{elas}}(P_i,\varepsilon_{ij}) + f_{\text{wall}}(P_{i,j}) + f_{\text{elec}}(P_i,E_i)]dV, \tag{2}$$

where V is the volume of the film and $dV=dx_1dx_2dx_3$. In this work, it is assumed that the strain field ε_{ij} and electric field E_i are always at equilibrium for a given polarization field distribution. The bulk free energy density of $PbTiO_3$ is described by a six-order Landau–Devonshire polynomial[15] with free energy coefficients collected from literature:[1,16] $\alpha_1=3.8(T-479)\times10^5$, $\alpha_{11}=-7.3\times10^7$, $\alpha_{12}=7.5\times10^8$, $\alpha_{111}=2.6\times10^8$, $\alpha_{112}=6.1\times10^8$, $\alpha_{123}=-3.7\times10^9$, $c_{11}=1.746\times10^{11}$, $c_{12}=7.937\times10^{10}$, $c_{44}=1.11\times10^{11}$, $Q_{11}=0.089$, $Q_{12}=-0.026$, $Q_{44}=0.0675$ (in SI units and T in °C). The contribution of domain walls to the total free energy is introduced through the polarization gradient, f_{wall}.

The elastic energy density is given by

$$f_{\text{elas}} = \frac{1}{2}c_{ijkl}e_{ij}e_{kl} = \frac{1}{2}c_{ijkl}(\varepsilon_{ij}-\varepsilon_{ij}^0)(\varepsilon_{kl}-\varepsilon_{kl}^0), \tag{3}$$

where $e_{ij}=\varepsilon_{ij}-\varepsilon_{ij}^0$ is the elastic strain, ε_{ij} is the total strain of the film compared to the parent paraelectric phase, and c_{ijkl} is

a)Electronic mail: shengguang@psu.edu.

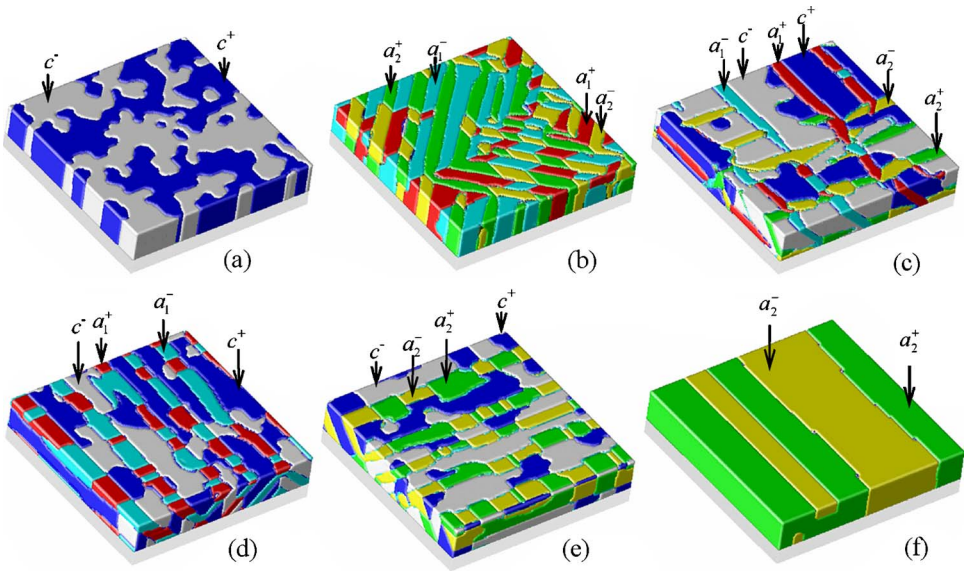

FIG. 1. (Color online) Domain morphologies in $PbTiO_3$ thin films under different anisotropic misfit strains: (a) c domain at $e_{s1}=e_{s2}=-0.010$; (b) a_1+a_2 domain at $e_{s1}=e_{s2}=0.015$; (c) $c+a_1+a_2$ domain at $e_{s1}=e_{s2}=0.005$; (d) $c+a_1$ domain at $e_{s1}=0.010$ and $e_{s2}=-0.010$; (e) $c+a_2$ domain at $e_{s_1}=-0.010$ and $e_{s2}=0.010$; (f) a_2 domain at $e_{s1}=-0.010$ and $e_{s2}=0.035$.

the elastic stiffness tensor. Both ε_{ij} and ε_{ij}^0 are defined using the cubic phase as the reference, and $\varepsilon_{ij}^0=Q_{ijkl}P_kP_l$ where Q_{ijkl} is the electrostrictive coefficient tensor. The details of the calculation of the total strain ε_{ij} in a (001)-oriented film under a biaxial strain are described in our previous publications.[3,10] In this work, the average film/substrate misfit strains $e_{s1}=\bar{\varepsilon}_{11}$ and $e_{s2}=\bar{\varepsilon}_{22}$ along x_1 and x_2 axes can be different because of a thermal mismatch and/or a lattice mismatch between a film and substrate. Here we assume $\bar{\varepsilon}_{12}=\bar{\varepsilon}_{21}=0$. The over bar indicates an average over the film.

The electrostatic energy density of a given polarization distribution was obtained by solving the electrostatic equilibrium equation under specified electric boundary conditions.[17,18] In the phase-field simulations, the temporal evolution of the polarization vector and thus the domain structures were obtained by numerically solving the TDGL using the semi-implicit Fourier-spectral method.[19] We employed $128\Delta x\times128\Delta x\times36\Delta x$ grid size, with periodic boundary conditions along the in-plane x_1 and x_2 axes. Δx is the spacing between two nearest grid points. The thickness of the film was taken as $h_f=20\Delta x$, and the region of the substrate allowed to deform is assumed be $h_s=12\Delta x$. Due to the lack of experimental data, an isotropic gradient energy coefficient G is chosen with a value of $G/G_0=0.6$ where G_0 is related to the magnitude of Δx through $\Delta x=\sqrt{G_{110}/\alpha_0}$ and $\alpha_0=|\alpha_1|_{T=25\,^\circ\mathrm{C}}$. The corresponding width of domain wall is about $1.5\Delta x$. The short-circuit boundary condition was employed to compute the dipole-dipole interactions.[20] We performed a series of simulations under anisotropic substrate/film misfit strains along x_1 and x_2 axes, ranging from −0.05 (compressive strain) to +0.05 (tensile strain). Each simulation proceeded for 20 000 time steps until the polarization distribution achieved steadiness.

III. RESULTS AND DISCUSSIONS

Examples of typical domain structures from our simulations are shown in Fig. 1 in which different domain variants are labeled. Figure 1(a) is a typical tetragonal domain structure under large compressive strains for both x_1 and x_2 directions ($e_{s1}=e_{s2}=-0.010$), in which there are two types of c domains of $(0,0,\pm P_3)$ separated by 180° domain walls. For the case with large tensile strains ($e_{s1}=e_{s2}=0.015$) along both x_1 and x_2 directions [Fig. 1(b)], only a_1 $(\pm P_1,0,0)$ and a_2 $(0,\pm P_2,0)$ twin domains exist. At intermediate strains, all three kinds of domains, c, a_1, and a_2, are present [Fig. 1(c)]. All the domain structures and domain wall orientation results are consistent with our previous simulations carried out under symmetric strains.[3,10]

The domain structures under anisotropic misfit strains can be significantly different compared to the symmetric case. Figure 1(d) shows a domain structure containing only c and a_1 domains for $e_{s1}=0.010$ and $e_{s2}=-0.010$, i.e., a tensile strain along x_1 direction and compressive strain along x_2. The a_1 domains are plates aligning about 45° from the film/substrate interface. As expected, $c+a_2$ domain structures are obtained when we reverse the strains along x_1 and x_2 axes ($e_{s1}=-0.010$ and $e_{s2}=0.010$), as shown in Fig. 1(e). The domain morphology is drastically different from the symmetric case of $e_{s1}=e_{s2}=0.010$ [Fig. 1(b)].

Figure 1(f) exhibits a domain structure under a very high strain anisotropy with a tensile strain along the x_2 direction $e_{s2}=0.035$ and the same compressive strain along the x_1 direction ($e_{s1}=-0.010$) as in Fig. 1(e). Compared with Fig. 1(e) which has $c+a_2$ domain structure, Fig. 1(f) contains only a_2 domains. The two types of a_2 domains $(0,\pm P_2,0)$ are separated by 180° domain walls. Similarly, only a_1 domains are present for $e_{s1}=0.035$ and $e_{s2}=-0.010$.

Based on the simulation results, a domain stability diagram, i.e., a representation of stable ferroelectric phases and domain structures as a function of misfit strains, is constructed under $T=25\,^\circ\mathrm{C}$ (Fig. 2). Under sufficiently large compressive strains, the stable state consists of pure c domains with 180° domain walls. A twin structure of a_1+a_2 domains is stable under relatively large tensile strains along both directions. The anisotropic strains (compressive strain at one direction and tensile strain at the other direction, vice versa) lead to either $c+a_1$ or $c+a_2$ domain structures. Purely a_1 or a_2 domain states are possible only under unrealistically large ($>\sim3.0\%$) compressive or tensile strain along either

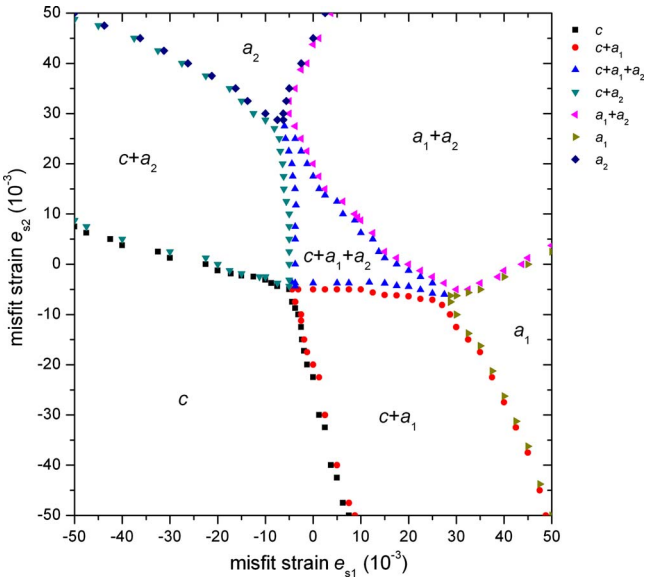

FIG. 2. (Color online) Misfit strain–misfit strain domain stability diagram for $PbTiO_3$ thin film at $T=25$ °C from phase-field simulation. Scattered symbols separating c, a_1, a_2, $c+a_1$, $c+a_2$, a_1+a_2, and $c+a_1+a_2$ phase regions.

one of the two in-plane directions. In the central part of the diagram, there is a stability region for the $c+a_1+a_2$ domain structure.

In Fig. 3, we compare the domain stability diagram (the red lines) using thermodynamic calculations assuming single domains for each ferroelectric state[11–14] and that from the phase-field simulations (scattered symbols as in Fig. 2). It is emphasized that the diagram from the phase-field approach is generated without any *a priori* assumption on the possible

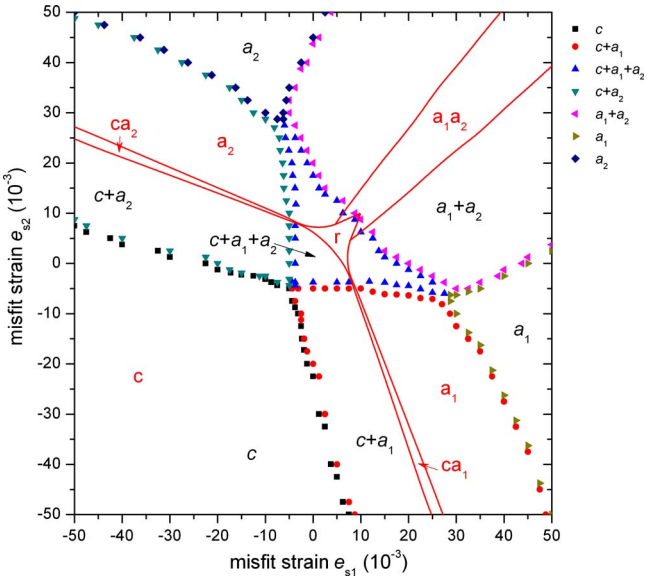

FIG. 3. (Color online) Misfit strain–misfit strain domain stability diagram for $PbTiO_3$ thin film at $T=25$ °C: Scattered symbols are phase boundaries from phase-field simulation separating c, a_1, a_2, $c+a_1$, $c+a_2$, a_1+a_2, $c+a_1+a_2$ phase regions, and solid lines are from thermodynamic calculations including (1) c phase ($P_1=P_2=0$, $P_3\neq 0$), (2) a_1 phase ($P_1\neq 0$ and $P_2=P_3=0$), (3) a_2 phase ($P_2\neq 0$ and $P_1=P_3=0$), (4) ca_1 phase ($P_1\neq 0$, $P_2=0$, $P_3\neq 0$), (5) ca_2 phase ($P_1=0$, $P_2\neq 0$, $P_3\neq 0$), (6) a_1a_2 phase ($P_1\neq 0$, $P_2\neq 0$, $P_3=0$), and (7) r phase ($P_1\neq 0$, $P_2\neq 0$, $P_3\neq 0$).

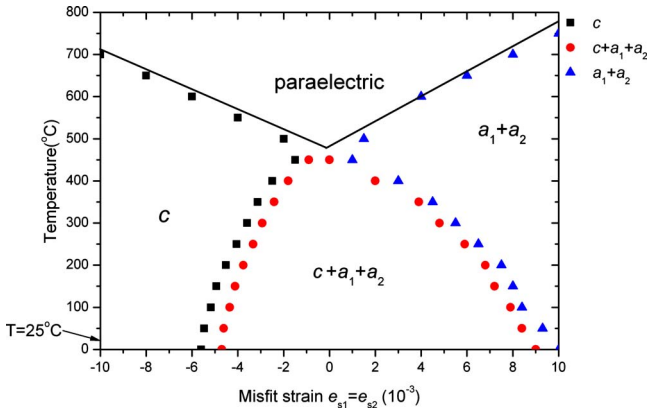

FIG. 4. (Color online) Misfit strain–temperature domain stability diagram for $PbTiO_3$ thin film under isotropic strains.

domain wall orientations. All the data points shown in Figs. 2 and 3 were obtained by starting from an initial paraelectric state. As a result, the a_1, a_2, or a_1+a_2 or $c+a_1$ or $c+a_2$ or $c+a_1+a_2$ domain configurations under different substrate constraints were automatically predicted using this approach. On the other hand, in the thermodynamic analysis,[11–14] the domain diagram (Fig. 3) containing c-phase, r-phase (P_1,P_2,P_3), a_1-phase$(P_1,0,0)$, a_2-phase$(0,P_2,0)$, ca_1-phase$(P_1,0,P_3)$, ca_2-phase$(0,P_2,P_3)$, or a_1a_2-phase $(P_1,P_2,0)$ was obtained under the same anisotropic substrate constraints using single-domain assumptions. As one can see in Fig. 3, the predicted diagram using phase-field simulations is not only quantitatively but also qualitatively different from that from thermodynamic calculations. First of all, all the new phases predicted by thermodynamic calculations, r, ca_1, ca_2, and a_1a_2 in Fig. 3, are artifacts resulted from the single-domain assumption. Second, thermodynamic calculations indicate that a moderate anisotropic strain of 1.0%, e.g., $e_{s1}=1.0\%$ and $e_{s2}=0.0$, would be sufficient to stabilize purely a_1 domains while phase-field simulations show that stabilizing purely a_1 or a_2 domains would require anisotropic strain levels (>3.0% along one of the two in-plane directions coupled with ~−1.0% along the other in-plane direction) that are unlikely to be achieved in real thin film growth processes. Finally, the stability field for purely c domains predicted by phase-field simulations is significantly narrower than that from thermodynamic calculations.

The isotropic ($e_{s1}=e_{s2}$) misfit strain–temperature domain stability diagram was also reproduced in Fig. 4. We noticed that although it is essentially the same as that we obtained previously,[3] there is a shift of the $c/c+a_1+a_2$ boundary, e.g., from $e_{s1}=e_{s2}=-0.010$ at 0 °C in Ref. 3 to around $e_{s1}=e_{s2}=-0.005$ in the present calculations. The boundary between the regions with $c+a_1+a_2$ domains and a_1+a_2 is around $e_{s1}=e_{s2}=0.010$ largely remains the same. The shift of the boundary between c domain and $c+a_1+a_2$ is caused by the fact that the electrostatic interactions in an inhomogeneous domain structure were ignored in the original work.[3] In the present calculation, a short-circuit boundary condition was assumed. The film surface charge is then compensated, and thus no depolarization field is produced. It should be noted that the polarization charges at the internal domain walls are

not entirely compensated and thus they can affect the volume fractions of different domain variants. The constant electrical potential on the surfaces promotes the formation of *c* domains,[17] leading to the enlargement of *c* domain region in Fig. 4.

IV. SUMMARY

In summary, a misfit strain–misfit strain phase/domain stability diagram was constructed for $PbTiO_3$ thin films at room temperature using phase-field simulations. It takes into account both elastic and electrostatic interactions under a short-circuit boundary condition. The predicted domain stability for anisotropic strains at room temperature is qualitatively different from those obtained using thermodynamic calculations based on the single-domain assumption.

ACKNOWLEDGMENTS

The authors are grateful for the financial support from the National Science Foundation (NSF) through Grant Nos. DMR-0205232 and DMR-0507146, Los Alamos National Laboratory, and from the Department of Energy under Grant No. DOE DE-FG02–07ER46417. The computer simulations were carried out on the LION clusters at the Pennsylvania State University supported in part by the NSF grants (Nos. DMR-9983532 and DMR-0122638) and in part by the Materials Simulation Center and the Graduate Education and Research Services at The Pennsylvania State University.

[1] N. A. Pertsev, A. G. Zembilgotov, and A. K. Tabantev, Phys. Rev. Lett. **80**, 1988 (1998).
[2] A. L. Roytburd, S. P. Alpay, V. Nagarajan, C. S. Ganpule, S. Aggarwal, E. D. Williams, and R. Ramesh, Phys. Rev. Lett. **85**, 190 (2000).
[3] Y. L. Li, S. Y. Hu, Z. K. Liu, and L. Q. Chen, Appl. Phys. Lett. **78**, 3878 (2001).
[4] N. A. Pertsev, V. G. Kukhar, H. Kohlstedt, and R. Waser, Phys. Rev. B **67**, 054107 (2003).
[5] C. M. Foster, G. R. Bai, R. Csencsits, J. Vetrone, R. Jammy, L. A. Wills, E. Carr, and J. Amano, J. Appl. Phys. **81**, 2349 (1997).
[6] S. K. Streiffer, J. A. Eastman, D. D. Fong, C. Thompson, A. Munkholm, M. V. Ramana Murty, O. Auciello, G. R. Bai, and G. B. Stephenson, Phys. Rev. Lett. **89**, 067601 (2002).
[7] V. Nagarajan, S. Prasertchoung, T. Zhao, H. Zheng, J. Ouyang, R. Ramesh, W. Tian, X. Q. Pan, D. M. Kim, C. B. Eom, H. Kohlstedt, and R. Waser, Appl. Phys. Lett. **84**, 5225 (2004).
[8] N. A. Pertsev and V. G. Koukhar, Phys. Rev. Lett. **84**, 3722 (2000).
[9] V. G. Koukhar, N. A. Pertsev, and R. Waser, Phys. Rev. B **64**, 214103 (2001).
[10] Y. L. Li, S. Y. Hu, Z. K. Liu, and L. Q. Chen, Acta Mater. **50**, 395 (2002).
[11] A. G. Zembilgotov, N. A. Pertsev, U. Bottger, and R. Waser, Appl. Phys. Lett. **86**, 052903 (2005).
[12] J. Wang and T. Y. Zhang, Appl. Phys. Lett. **86**, 192905 (2005).
[13] J. H. Qiu and Q. Jiang, J. Appl. Phys. **101**, 034110 (2007).
[14] J. Wang and T. Y. Zhang, Phys. Rev. B **77**, 014104 (2008).
[15] A. F. Devonshire, Philos. Mag. **3**, 85 (1954).
[16] M. J. Haun, E. Furman, S. J. Jang, H. A. Mckinstry, and L. E. Cross, J. Appl. Phys. **62**, 3331 (1987).
[17] Y. L. Li, S. Y. Hu, Z. K. Liu, and L. Q. Chen, Appl. Phys. Lett. **81**, 427 (2002).
[18] Y. L. Li, L. Q. Chen, G. Asayama, D. G. Schlom, M. A. Zurbuchen, and S. K. Streiffer, J. Appl. Phys. **95**, 6332 (2004).
[19] L. Q. Chen and J. Shen, Comput. Phys. Commun. **108**, 147 (1998).
[20] Y. L. Li, S. Y. Hu, and L. Q. Chen, J. Appl. Phys. **97**, 034112 (2005).